THE JOURNAL OF BIOLOGICAL CHEMISTRY VOL. 284, NO. 33, pp. 22390–22400, August 14, 2009

Structural Insights into the Acyl Intermediates of the *Plasmodium falciparum* Fatty Acid Synthesis Pathway

THE MECHANISM OF EXPANSION OF THE ACYL CARRIER PROTEIN CORE[*S]

Received for publication, February 26, 2009, and in revised form, June 10, 2009 Published, JBC Papers in Press, June 11, 2009, DOI 10.1074/jbc.M109.014829

Santosh Kumar Upadhyay[‡1], **Ashish Misra**[§1], **Richa Srivastava**[§], **Namita Surolia**[¶2], **Avadhesha Surolia**[‡§3], **and Monica Sundd**[‡4]

From the [‡]*National Institute of Immunology, New Delhi 110067, the* [§]*Molecular Biophysics Unit, Indian Institute of Science, Bangalore 560012, and the* [¶]*Molecular Biology and Genetics Unit, Jawaharlal Nehru Center for Advanced Scientific Research, Bangalore 560064, India*

Acyl carrier protein (ACP) plays a central role in fatty acid biosynthesis. However, the molecular machinery that mediates its function is not yet fully understood. Therefore, structural studies were carried out on the acyl-ACP intermediates of *Plasmodium falciparum* using NMR as a spectroscopic probe. Chemical shift perturbation studies put forth a new picture of the interaction of ACP molecule with the acyl chain, namely, the hydrophobic core can protect up to 12 carbon units, and additional carbons protrude out from the top of the hydrophobic cavity. The latter hypothesis stems from chemical shift changes observed in C_α and C_β of Ser-37 in tetradecanoyl-ACP. $^{13}C,^{15}N$-Double-filtered nuclear Overhauser effect (NOE) spectroscopy experiments further substantiate the concept; in octanoyl (C_8)- and dodecanoyl (C_{12})-ACP, a long range NOE is observed within the phosphopantetheine arm, suggesting an arch-like conformation. This NOE is nearly invisible in tetradecanoyl (C_{14})-ACP, indicating a change in conformation of the prosthetic group. Furthermore, the present study provides insights into the molecular mechanism of ACP expansion, as revealed from a unique side chain-to-backbone hydrogen bond between two fairly conserved residues, Ile-55 HN and Glu-48 O. The backbone amide of Ile-55 HN reports a pK_a value for the carboxylate, ~1.9 pH units higher than model compound value, suggesting strong electrostatic repulsion between helix II and helix III. Charge-charge repulsion between the helices in combination with thrust from inside due to acyl chain would energetically favor the separation of the two helices. Helix III has fewer structural restraints and, hence, undergoes major conformational change without altering the overall-fold of *P. falciparum* ACP.

In the malarial parasite *Plasmodium falciparum,* fatty acid biosynthesis occurs by a pathway distinct from the host. A number of enzymes involved in the process *viz.* β-ketoacyl acyl carrier protein (ACP)[5] synthase III, β-hydroxy acyl-ACP hydratase, and enoyl-ACP reductase are targets for drug design (1, 2). An indispensable component, crucial for each step of the pathway, is a small acidic protein, the ACP. ACP plays a pivotal role in a range of biochemical processes, like fatty acid biosynthesis (3), polyketide synthesis (4, 5), oligosaccharides (6), biotin, and nonribosomal peptide synthesis (7, 8). Thus, the knowledge of structural features, which dictate ACP function, could offer new avenues for inhibitor design to disable several pathways of the parasite in parallel.

Acyl carrier protein differs structurally in the host and the parasite. It exists as an independent protein in type II fatty acid synthesis pathway, observed in *P. falciparum*, *Escherichia coli*, spinach, and most prokaryotes. In the type II pathway, fatty acids are synthesized by multiple enzymes catalyzing different reactions. Conversely, mammalian ACP (malarial host) is an integral domain of one single multidomain, multifunctional fatty acid synthase (FAS) (type I pathway), each domain catalyzing a particular reaction. Interestingly, ACPs of type I and II pathway share a similar fold, the ACP molecule of type II pathway can be substituted with the ACP domain of type I pathway in some cases, and the latter is recognized as a substrate *in vitro* by key enzymes of type II pathway (9).

The primary function of ACP is to shuttle the lengthening acyl chains to the catalytic site of FAS enzymes. It is expressed as an apoprotein (inactive) and modified to holo-ACP (active) by the transfer of a 4′-phosphopantetheine moiety from coenzyme A (CoA) to a conserved serine residue, Ser-36/37, with ACP synthase acting as a catalyst. The acyl chain gets covalently tethered to the terminal cysteamine thiol of the 4′-phosphopantetheine prosthetic group, which in turn transfers the acyl chain to the respective enzymes during elongation. Biosynthesis of fatty acid(s) is initiated by the carboxylation of acetyl-CoA to malonyl-CoA, which is transacylated to malonyl-ACP. Malonyl-ACP condenses with acetyl-CoA, resulting in the formation of enoyl-/butyryl-ACP (C_4-) which enters the elongation

* This work was supported through the NMR Facility at the National Institute of Immunology, New Delhi, supported by the Department of Biotechnology, Government of India.

[S] The on-line version of this article (available at http://www.jbc.org) contains supplemental Table 1.

[1] Both authors contributed equally to this work.

[2] A J. N. Tata Innovation Fellow of the Department of Biotechnology.

[3] To whom correspondence may be addressed: National Institute of Immunology, Aruna Asaf Ali Marg, JNU Campus, New Delhi 110 067, India. Tel.: 91-11-26717102/26717103; Fax: 91-11-26717104; E-mail: surolia@nii.res.in.

[4] To whom correspondence may be addressed: National Institute of Immunology, Aruna Asaf Ali Marg, JNU Campus, New Delhi 110 067, India. Tel.: 91-11-26703823; Fax: 91-11-26162125; E-mail: monicasundd@nii.res.in.

[5] The abbreviations used are: ACP, acyl carrier protein; PfACP, *P. falciparum* ACP; FAS, fatty acid biosynthesis; HSQC, heteronuclear single quantum coherence spectroscopy; TOCSY, total correlation spectroscopy; CoA, coenzyme A; NOESY, nuclear Overhauser effect (NOE) spectroscopy.

cycle. Two carbon atoms are added per elongation cycle, resulting in acyl-ACPs C_6-, C_8-, C_{10}-, C_{12}-, C_{14}-, and C_{16}-ACP. Palmitate (C_{16}) is the most common product of type I pathway, whereas in the type II pathway, products range from saturated to unsaturated, branched, unbranched, or variable chain lengths.

Structurally, ACP is a four-helix bundle protein, with the helices enclosing a central hydrophobic cavity (10–17). In the type II pathway, the hydrophobic cavity accommodates the growing acyl chain and the β-mercaptoethyl moiety of the 4′-phosphopantetheine arm. The acyl chain remains embedded in the cavity, which expands with increasing length of the acyl chain as observed in *E. coli* and spinach (12). The mechanism of acyl chain interaction with the ACP molecule is remarkably different in rat, which belongs to the type I fatty acid pathway. Insignificant interactions between the ACP molecule and the acyl chain are observed, suggesting that the ACP molecule does not sequester the acyl chain, and therefore, the acyl chain in type I pathway is protected in a way different from the type II pathway (18).

Despite the availability of structural data for a number of acyl-ACPs *e.g. E. coli* and spinach (12, 14, 19, 20), molecular details pertaining to acyl chain carriage and its presentation to the FAS enzymes of type II pathway is still an enigma. The general consensus is that the ACP molecule can accommodate 10 carbon atoms only. In spinach, the hydrophobic cavity of ACP expands to accommodate acyl chain lengths ranging from $C_{10:0}$ to $C_{18:0}$. However, chains longer than 10 carbon units are not fully protected (14). In *E. coli*, 10 carbon atoms have been observed to be accommodated in the hydrophobic core (19). A molecular dynamics study on *E. coli* published recently also shows that the hydrophobic core of ACP can hold a maximum of 10 carbon atoms only (21). Here, we demonstrate that *P. falciparum* ACP (PfACP) can protect more than 10-carbon-atom-long acyl chains, with a maximum of 12 carbon atoms. An *in silico* study on PfACP published recently proposes the possible mechanism of substrate delivery based on steered molecular dynamics simulations using *E. coli* acyl-ACPs as the starting model (22). There are no experimental data (x-ray or NMR) available to date on the acyl-ACPs of *P. falciparum.* Present work for the first time provides structural insights into the acyl-PfACP intermediates using NMR as a primary tool. The precision and sensitivity of NMR allowed identification of key interactions between the acyl chain and the ACP molecule, leading to the proposal of a model unraveling the sequence of structural changes accompanying acyl chain insertion. The molecular basis of ACP expansion in PfACP upon acyl chain elongation has also been deciphered.

EXPERIMENTAL PROCEDURES

Cloning, Expression, and Purification—Cloning, expression, and purification of *P. falciparum* holo-ACP in *E. coli* has already been described (23). *E. coli* holo-ACP synthase, apoPfACP and respective acyl-CoAs were used for the synthesis of butyryl-, octanoyl-, decanoyl-, dodecanoyl-, tetradecanoyl-, and hexadecanoyl-ACP using a modified protocol of Lambalot and Walsh (24) as described (23). Uniformly labeled ^{13}C, ^{1}H,^{15}N-apoACP was prepared by growing *E. coli* in M9 media containing ^{15}N NH_4Cl (1 g/liter) and ^{13}C glucose (2 g/liter) (Spectra Stable Isotopes). The N-terminal His tag was removed by thrombin cleavage.

NMR Spectroscopy—NMR samples were comprised of uniformly labeled ^{13}C, ^{1}H,^{15}N protein in 50 mM sodium phosphate buffer, pH 6.5, 100 mM NaCl, 2 mM dithiothreitol, 0.5% sodium azide, 90% H_2O, and 10% D_2O. A protein concentration of 1 mM was used throughout. The phosphopantetheine arm and the acyl chains were unlabeled, as the proteins were synthesized by enzymatic modification of uniformly labeled ACP.

Two- and three-dimensional NMR experiments, *viz.* $^{1}H^{15}N$ HSQC, $^{1}H^{15}N$ TOCSY, HNCACB, CBCAcoNH, CCcoNH, HNcoCA, and $^{13}C^{15}N$-filtered experiments were acquired on a Varian Inova 500, installed at the National Institute of Immunology, New Delhi, India, equipped with a triple resonance, Z-pulsed field gradient probe. Experiments were performed at 300 K. NMR data were processed on a work station running Red Hat Enterprize Linux 5.0, using NMRPipe/NMRDraw (25) and analyzed using Sparky (26). The data were multiplied by a phase shifted sinebell apodization function in all dimensions.

$^{1}H^{15}N$ HSQC spectra were acquired using 1024 data points (t2) dimension and 512 data points (t1) dimension. $^{1}H^{15}N$ HSQC-TOCSY experiments were collected with 1024 (t3) × 72 (t1) × 48 (t2) data points and a mixing time of 150 ms. CBCAcoNH, HNCACB, and CCcoNH experiments were collected with 1024 (t3) × 36 (t1) × 24 (t2) data points. Data were linear-predicted in the forward direction for up to half the number of experimental points in the indirect dimensions. In $^{13}C^{15}N$-filtered two-dimensional NOESY experiments, a mixing time of 400 ms was used with 1024 data points in the t2 dimension and 1024 points in the t1 dimension. In ^{13}C-filtered ^{15}N-edited triple resonance NOESY experiments, a mixing time of 300 ms with 1024 (t3) × 48 (t1) × 24 (t2) data points were used.

Data Analysis—Changes in HN have been reported as average chemical shifts ($\Delta\Delta\delta_{HN}$) derived from the equation

$$\Delta\Delta\delta_{HN} = [(\Delta_{HN})^2 + (\Delta N/5)^2]^{1/2} \quad \text{(Eq. 1)}$$

where Δ_{HN} is the change in chemical shift in the proton dimension, and ΔN is the change in chemical shift in the nitrogen dimension.

All chemical shift changes reported in the study ΔHN, ΔC_α, and ΔC_β are differences in chemical shift of a given acyl-ACP and the preceding acyl intermediate, *i.e.* butyryl (butyryl-holo-)-, octanoyl (octanoyl-butyryl)-, decanoyl (decanoyl-octanoyl)-, dodecanoyl (dodecanoyl-decanoyl)-, tetradecanoyl (tetradecanoyl-dodecanoyl)-, and hexadecanoyl (hexadecanoyl-tetradecanoyl)-ACP. One standard deviation has been used as a cutoff to demarcate significant chemical shift change and is represented as a discontinuous horizontal line in the figures.

pK_a Determination—pH titration studies were carried out in the pH range 8.0-3.5. Protein samples were comprised of 1 mM holo-ACP, 0.1 M KCl, 90% H_2O, 10% D_2O, and 2 mM dithiothreitol. Sodium 4,4-dimethyl-4-silapentanesulfonate was used as an internal standard. Apparent pK_a value for the backbone amide was obtained by fitting proton chemical shifts *versus* pH to the modified Hill equation (27, 28),

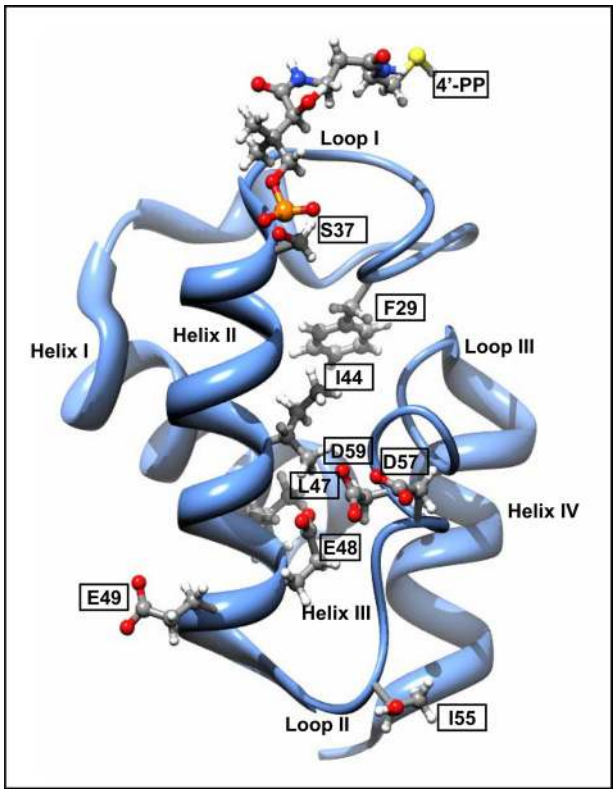

FIGURE 1. **Structure of holo-PfACP with some of the residues that interact with the acyl chain shown in *ball and stick*.** The structure is based on the NMR structure of *P. falciparum* holo-ACP, PDB ID 2FQO. The prosthetic group (*4′-PP*) attached to Ser-37 is also shown in *ball and stick*. The figure was prepared using UCSF-Chimera (43).

$$\delta_{obs} = \delta_A[1 + 10^{n(pK_a - pH)}]^{-1} + \delta_{HA}[1 - (1 + 10^{n(pK_a - pH)})^{-1}] \quad \text{(Eq. 2)}$$

where δ_{obs} is the observed chemical shift at a given pH, δ_A andδ_{HA} are the chemical shifts of fully deprotonated and protonated species, respectively, and n is the Hill coefficient, a measure of cooperativity.

RESULTS

Acyl Interaction Surface of the ACP Molecule—The NMR structure of holo-PfACP comprises four helices surrounding a central hydrophobic cavity, helix I (residues 4–15), helix II (residues 37–51), helix III (residues 57–60), and helix IV (residues 66–75) (14). A phosphopantetheine moiety attaches to the side chain OH of Ser-37, as shown in Fig. 1. The other end of phosphopantetheine moiety is subsequently attached to the acyl chain by a thioester bond, resulting in the formation of acyl-ACP intermediates. In *P. falciparum*, a range of acyl-ACPs is formed during fatty acid biosynthesis, the primary products being $C_{10:0}$, $C_{12:0}$, and $C_{14:0}$-ACPs (29–31). The molecular mechanism by which the acyl chain is carried by the PfACP molecule and the structural changes accompanying acyl chain elongation in ACP remain unknown. In this study we have simulated the process of fatty acid biosynthesis in *P. falciparum* by synthesizing a range of acyl-ACP intermediates and studying them using NMR. Butyryl (C_4)-, octanoyl (C_8)-, decanoyl (C_{10})-, dodecanoyl (C_{12})-, and tetradecanoyl (C_{14})-ACP have been studied along with holo-ACP, the active form of ACP that participates in the initiation of fatty acid biosynthesis. Hexadecanoyl-ACP (C_{16} or palmitate) has also been included in this study despite not being physiologically relevant to extrapolate the data to systems synthesizing longer fatty acids. All acyl intermediates were synthesized *in vitro* by enzymatic processing of ^{13}C,^{15}N-labeled apoACP. Therefore, only the ACP molecule was ^{13}C,^{15}N-labeled, with the prosthetic group and the acyl chain remaining unlabeled.

Holo-ACP chemical shifts were assigned based on the Biological Magnetic Resonance Bank entry 6516,(15), whereas peaks in the acyl intermediates were assigned by analyzing three-dimensional NMR experiments *viz.* $^1H^{15}N$ TOCSY, CBCAcoNH, HNCACB, and HNcoCA. HN chemical shifts have been presented as average of changes in ^1H and ^{15}N dimension, as perturbations were observed in both dimensions. All chemical shift changes reported in this manuscript (HN, C_α, C_β) are relative changes between a given acyl-ACP and the preceding acyl intermediate (one with smaller acyl chain length) as described under "Experimental Procedures." A S.D. $> 1\ \sigma$ has been used to define significant chemical shift change and is represented as a *dotted line* in Figs. 2 and 3. Fig. 2, *A–F*, illustrates the average chemical shift change (ΔHN_{avg}) for the backbone amides in the acyl-ACPs.

Chemical shift perturbation study is a highly sensitive approach, and hence, the slightest changes in conformation as a result of ligand interaction can be ascertained. In butyryl-ACP, a change in chemical shift for residues present in loop I, helix II, loop II, and loop III is observed (Fig. 2*A*). The amides of Phe-29, Thr-30, Ser-37, Leu-38, Ile-55, and Leu-61 display a noticeable change in chemical shift.

Octanoyl-ACP causes a change in chemical shift for residues in loop I, helix II, loop II, helix III, loop III, and helix IV (Fig. 2*B*). Some of the residues displaying large chemical shift changes are Phe-29, Thr-30, Ala-35, Leu-38, Met-45, Ile-55, and Gln-67. Decanoyl-ACP induces marked chemical shift change in residues localized primarily in loop II, *i.e.* Val-53, Thr-54, and Ile-55. Conversion of decanoyl- to dodecanoyl-ACP is accompanied with a change in chemical shift of the amides in helix I, helix II, loop II, helix III, and helix IV. Tetradecanoyl-ACP shows very little change, except for a couple of residues, Val-53 and Ile-55. Changes in hexadecanoyl-ACP were insignificant in comparison to other acyl-ACPs as shown in Fig. 2*F*. Ile-55 HN could not be traced in hexadecanoyl-ACP due to signal overlap and, therefore, is not included in the figure.

Maximum chemical shift change was observed in dodecanoyl-ACP, and least perturbed were the amides in hexadecanoyl-ACP. Because of signal overlap, we have excluded Asp-39 and Leu-40 in all our studies. It is intriguing that most of the residues that report significant change in backbone amide chemical shift are hydrophobic in nature or the ones adjoining a hydrophobic residue. The pattern of chemical shift change demonstrates the nature of acyl-ACP interaction; the acyl chain is lodged in the hydrophobic cavity, and consequently, overall expansion of the molecule ensues to accommodate the acyl chain. The observation of relatively small chemical shift changes upon conversion of dodecanoyl- to tetradecanoyl- or hexadecanoyl-ACP suggests that the hydrophobic cavity of

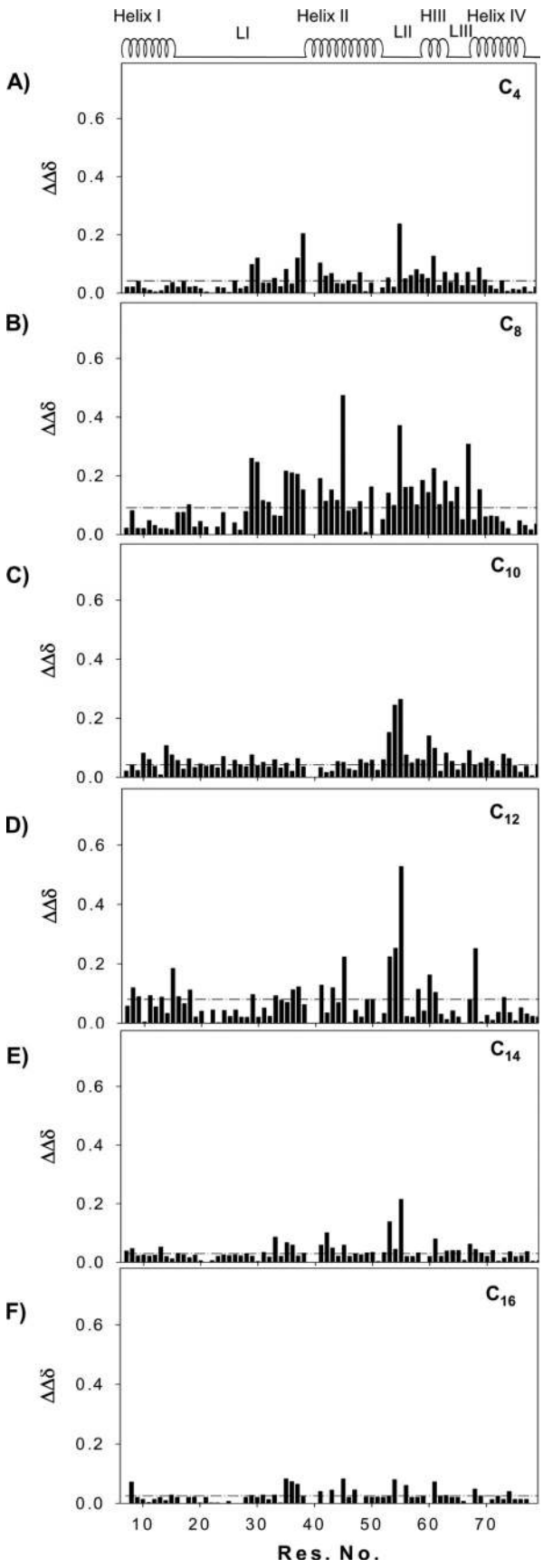

FIGURE 2. **Average chemical shift changes (ΔHN_{avg}) of the backbone amides.** Changes in average chemical shift of the acyl-ACP intermediates butyryl (C_4)-, octyl (C_8)-, decanoyl (C_{10})-, dodecanoyl (C_{12})-, tetradecanoyl (C_{14})-, and hexadecanoyl (C_{16})-ACP are shown. Average chemical shifts were calculated from changes in ΔH and ΔN using Equation 1 and are reported in ppm.

PfACP can accommodate acyl chains up to 12 carbon atoms only and, thereafter, any carbon atom added is not completely protected by the hydrophobic core. Minor changes in chemical shift in the neighborhood of Ile-55 and Ser-37 reflect the strain within the ACP molecule to accommodate maximal number of hydrophobic carbons.

Changes in Backbone C_α Conformation—C_α chemical shift is a benchmark of any change in protein fold or backbone. An advantage of C_α chemical shift over backbone amides is their insensitivity to hydrogen-bond interactions, and therefore, the extent of chemical shift perturbation is directly proportional to conformational change. Fig. 3, *A–E*, shows the changes in C_α chemical shift of the acyl-ACP intermediates.

In butyryl-ACP, backbone C_α chemical shift changes are observed in Phe-29, Ser-37, Leu-40, Ile-44, Lys-62, and Ile-63 (Fig. 3*A*). Octanoyl-ACP formation is accompanied with changes in a few other residues as well, Asp-6, Ala-46, Leu-47, and Ile-55, in addition to Phe-29, Ile-44, Lys-62, and Ile-63, which display a C_α change in butyryl-ACP. Phe-29 shows a 3-fold change in chemical shift in octanoyl- compared with butyryl-ACP, whereas Ile-44 changes 2-fold. Decanoyl-ACP formation is accompanied with a change in chemical shift of residues Thr-54, Ile-55, and Ser-56 in loop II, Gln-58 and Asp-59 in helix III, Leu-61 and Ile-63 in loop III, and Val-66, Gln-67, Ile-73, and Glu-74 in helix IV. Apart from these, a few other residues also display a change in chemical shift, Ile-12 in helix I, Ser-27 in the loop I, and Leu-47 in helix II, as shown in Fig. 3*C*. Notably, Leu-47, Ile-55, and Ile-63 that display a change in C_α chemical shift in octanoyl-ACP undergo a further change in decanoyl-ACP.

Conversion of decanoyl- to dodecanoyl-ACP induces a change in chemical shift for residues present in helix II (Leu-47 and Phe-51, loop II; Val-53, loop III; Leu-61 and Lys-62) and helix IV (Ile-73) as shown in Fig. 3*D*. Ile-73 displays maximum C_α change in dodecanoyl-ACP, *i.e.* ~1.01 ppm. The C_α of Leu-47 is seen undergoing a chemical shift change consistently in octanoyl-, decanoyl-, and dodecanoyl-ACP, although major change occurs only in dodecanoyl-ACP. Changes in C_α for Ser-37 and a few residues in the neighborhood of Ile-55 are observed in tetradecanoyl-ACP. Data for hexadecanoyl-ACP could not be acquired due to high rate of thioester bond hydrolysis, a pace much faster than NMR time scale.

Fig. 4 highlights the regions in acyl-PfACPs undergoing conformational change. The extent of swelling in a given acyl-ACP is directly proportional to C_α chemical shift change. Some of the residues displaying significant C_α chemical shift change are shown in *ball and stick*. A *green arrow* shown on the *right side* of the figure along with a *number* indicates the length of the acyl chain buried in the hydrophobic cavity. The *red colored bar* denotes the region that gets exposed to the solvent. In butyryl-ACP, chemical shift changes are confined to helix I, loop II, and a small part of loop III, close to the top opening of the hydrophobic cavity. In octanoyl-ACP, the acyl chain penetrates deep in the cavity, and hence, chemical shift perturbation moves to

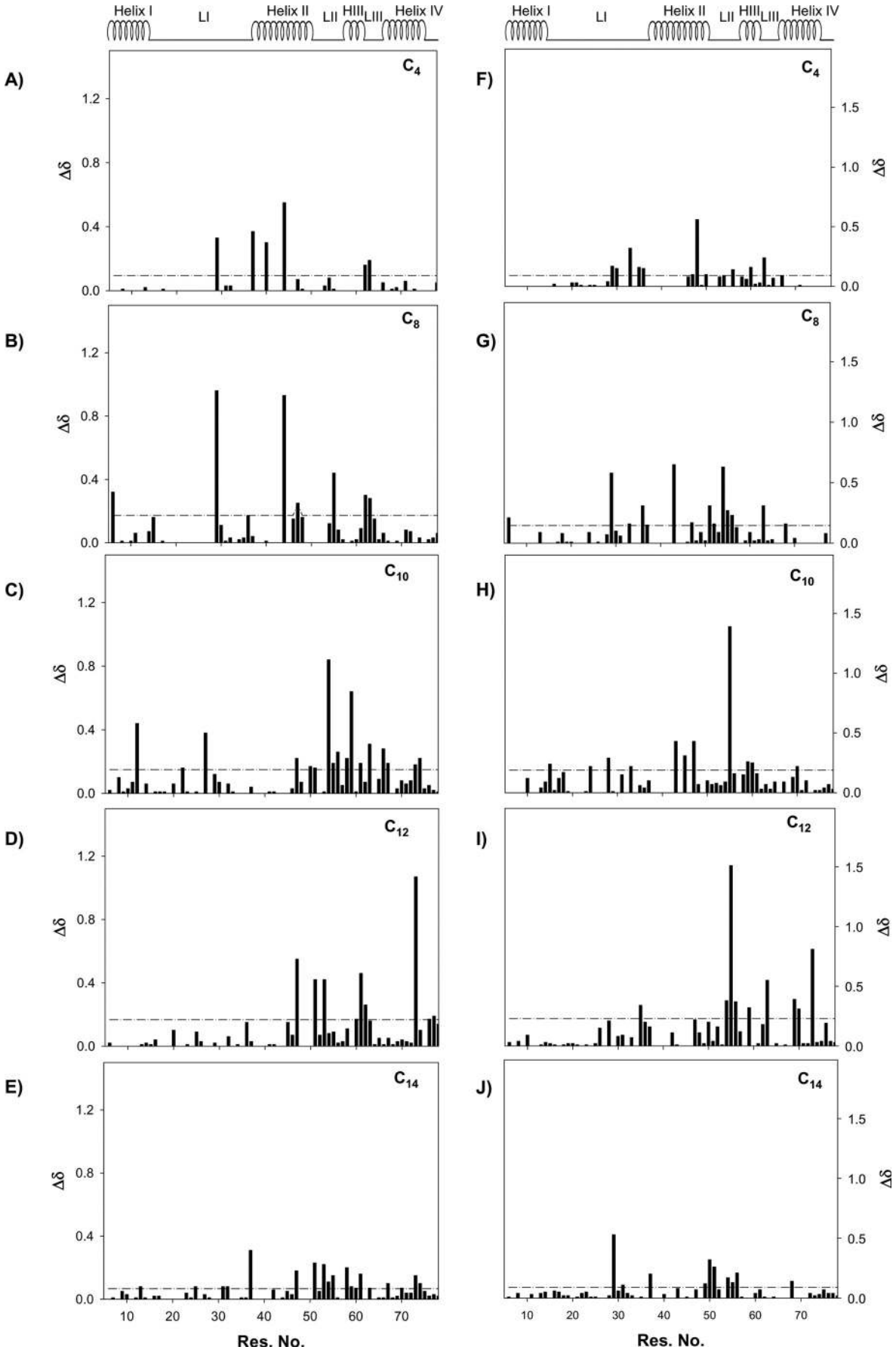
Helix I
LI
Helix II
LII
HIII
LIII
Helix IV
A)
B)
C)
D)
E)
F)
G)
H)
I)
J)
C_4
C_8
C_{10}
C_{12}
C_{14}
Δδ
Res. No.

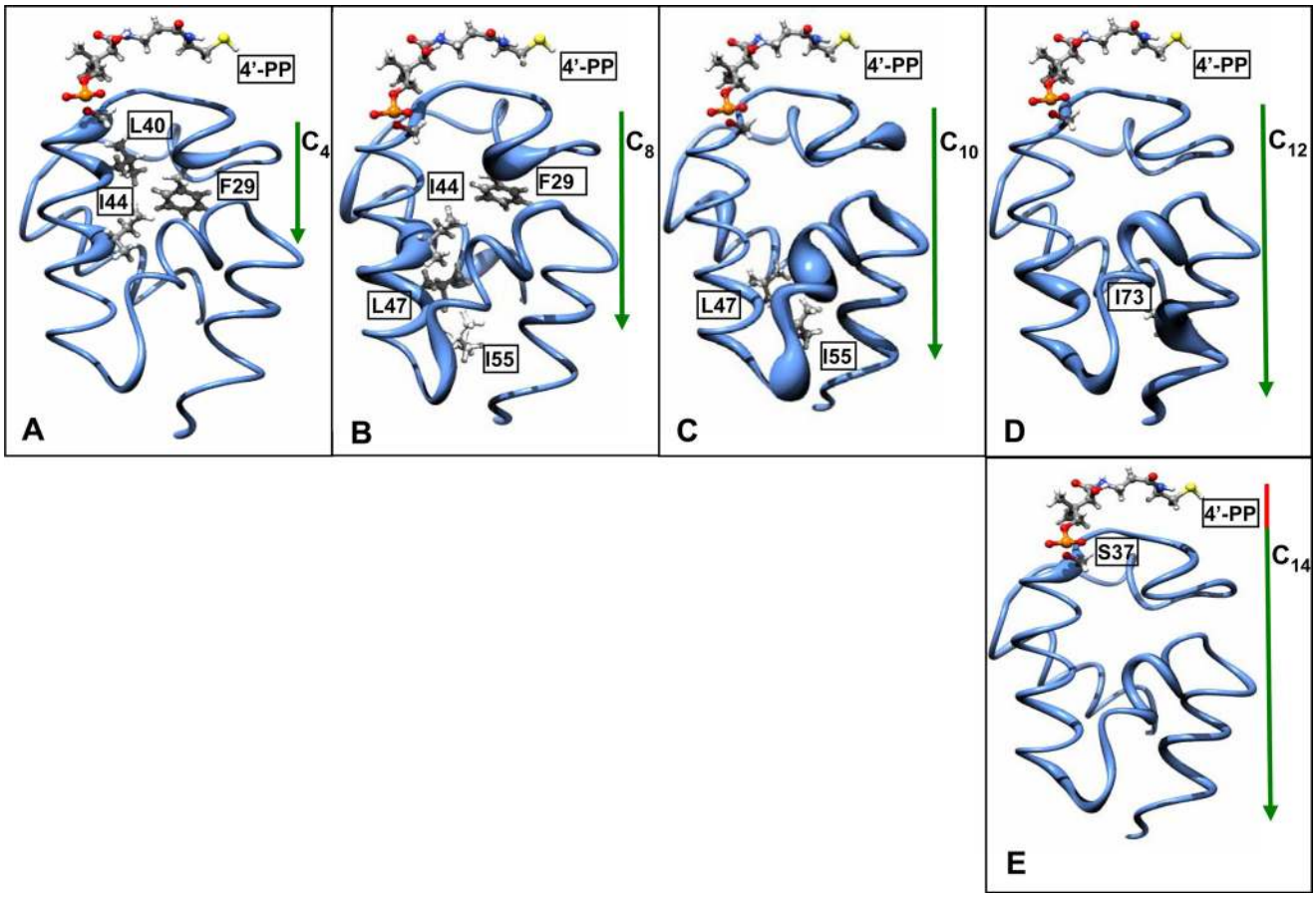

FIGURE 4. **Structural changes in the C_α backbone of the acyl-PfACPs.** Worm representation of C_α chemical shift changes in the ACP backbone in butyryl (*A*)-, octyl (*B*)-, decanoyl (*C*)-, dodecanoyl (*D*)-, and tetradecanoyl (*E*)-ACP. Thickness of the worm at every given point is directly proportional to C_α chemical shift change. The *green arrow* on the *right* and a *number* adjacent to it indicates the extent of acyl chain insertion into the ACP molecule. The *red bar* shows the region of the acyl chain that is not completely protected by the hydrophobic core. The figure was prepared using UCSF Chimera (43).*4′-PP*, 4′-phosphopantetheine.

the lower half of helix II and loop II. In decanoyl-ACP, changes occur in loop II, helix III, loop III, and helix IV. In dodecanoyl-ACP, helix II, loop II, loop III, and the lower part of helix IV undergo conformational change. Perturbation of helix IV at the C terminus in dodecanoyl-ACP indicates slight widening of the bottom opening of the hydrophobic core. Taken together, maximum C_α change occurs in helix III during acyl chain elongation and is observed in decanoyl-ACP.

Side Chain Rearrangements—C_β chemical shifts are reporters of side-chain conformation and, hence, offer excellent opportunities to follow side-chain rearrangement upon ligand interaction. Fig. 3, *F–J*, illustrates the changes in C_β of PfACP as a function of acyl chain growth. In butyryl-ACP, residues Phe-29, Thr-30, Leu-33, Ala-35, Asp-36, Glu-48, Ser-56, and Ile-63 display a significant change in chemical shift. Changes in C_β of Phe-29 and Ile-63 are consistent with changes in C_α. In octanoyl-ACP, Asp-6, Phe-29, Asp-36, Leu-43, Leu-47, Phe-51, Asn-52, Thr-54–Ser-56, Ile-63, and Asp-68 experience a chemical shift change $>1\sigma$ S.D. Decanoyl-ACP is accompanied with a chemical shift change of Gln-15, Gln-24, Asn-28, Leu-33, Leu-43, Met-45, Leu-47, Ile-55, Asp-59, and Ala-60. In dodecanoyl-ACP, residues Ala-35, Thr-54–Ser-56, Asp-59, Ile-63, Ala-69, Ile-70, and Ile-73 show a large change in C_β chemical shift. In tetradecanoyl-ACP, changes in C_β are relatively small compared with other ACPs. Only a slight change in Phe-29, Ser-37, Lys-50, Phe-51, and Thr-54–Ser-56 is observed. Residues between Lys-50–Ser-56 are localized at the bottom of the hydrophobic cavity, whereas Ser-37 is attached to the acyl chain, and it resides outside the cavity in helix II. Thus, observed C_β chemical shift changes occur either for residues that are indirectly attached to the acyl chain or present at the openings of the hydrophobic cavity. Overall, three residues display large changes in side-chain conformation as the acyl chain grows from holo- to tetradecanoyl-ACP; Phe-29 by 0.75 ppm, Ile-55 by 1.51 ppm, and Ile-73 by 0.81 ppm.

Putative Side Chain to Backbone Hydrogen Bond—Backbone amides are good reporters of hydrogen bonds, and proton chemical shifts depend on the inverse third power of the distance between amide proton and hydrogen bond acceptor. Therefore, changes in HN report not only direct interaction of a ligand with the backbone amide but also stretching/skewing of hydrogen bonds. It has been shown by other studies that a

FIGURE 3. **C_α and C_β chemical shift changes.** Shown are plots illustrating C_α chemical shift changes in butyryl- (*A*), octanoyl- (*B*), decanoyl- (*C*), dodecanoyl- (*D*), tetradecanoyl-ACP (*E*) and C_β chemical shift changes in butyryl- (*F*), octanoyl- (*G*), decanoyl- (*H*), dodecanoyl- (*I*), and tetradecanoyl-ACP (*J*) upon acyl chain elongation. Chemical shift changes are reported in ppm.

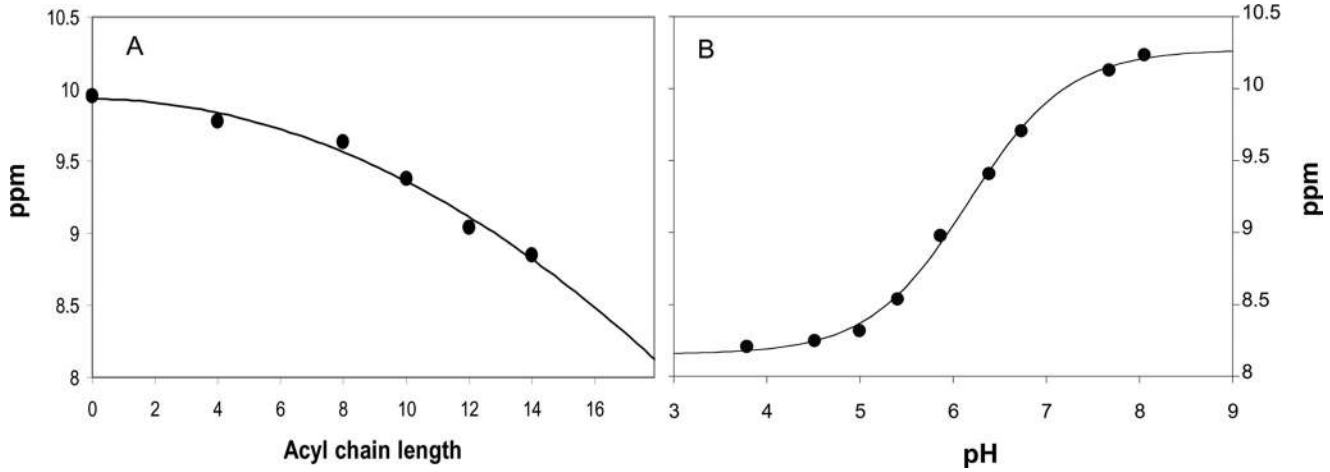

FIGURE 5. **Changes in chemical shift of Ile-55 HN.** Changes in Ile-55 HN chemical shift as a function of acyl chain length (*A*) (the data have been fitted to a second order polynomial) and pH (*B*) are shown. The apparent pK_a value was obtained by fitting HN chemical shift to a modified Hill equation (Equation 2). Chemical shift changes were obtained from $^{1}H^{15}N$ HSQC spectra.

backbone amide hydrogen bonded to a side-chain carboxylate displays a chemical shift change >1 ppm, and its apparent pK_a value matches with that of the carboxyl group accepting the hydrogen bond (27, 28, 32). The apparent pK_a value reported by the amide is usually within 0.1–0.2 units of the pK_a of the carboxylate.

Based on a large upfield chemical shift change of the backbone amide (δΔHN) upon acyl chain elongation and close proximity of the HN to a polar side chain <5 Å in the NMR structure, we have identified a putative hydrogen bond between the backbone amide of Ile-55 HN and the side chain oxygen of Glu-48. In the NMR structure of PfACP, Glu-48 is present at the bottom of helix II with its side chain stretching toward loop II, whereas Ile-55 is localized in loop II; the distance between the carbonyl oxygen of Glu-48 and the carbonyl N of Ile-55 is <3.8 Å in one of the models of the ensemble. Ile-55 HN has a downfield chemical shift value of 9.95 ppm in holo-ACP, which shifts upfield by more than 1.1 ppm upon the addition of 14 carbon atoms. Fig. 5*A* shows the changes in chemical shift of Ile-55 HN as a function of carbon chain length.

A pH titration study carried out on the PfACP molecule in the pH range 8.0-3.5 (the range over which the PfACP molecule is stable) further confirmed the presence of a hydrogen bond. The change in chemical shift of Ile-55 HN as a function of pH is shown in Fig. 5*B*. Data have been fitted to a modified Hill equation (Equation 2) to obtain the pK_a value. The chemical shift of Ile-55 HN changes from 10.27 ppm at pH 8.1 to 8.16 ppm at pH 3.8, *i.e.* ~2 ppm upfield, reporting an apparent pK_a of 6.16 ± 0.04 for Glu-48. A Hill coefficient of 0.81 was obtained from the fit.

Conformation of the Phosphopantetheine Moiety—$^{13}C,^{15}N$-Double-filtered NOESY experiments were acquired to understand the conformational differences between the phosphopantetheine arm in the acyl-PfACPs. As shown in Fig. 6*A*, most of the NOEs observed for the prosthetic group are short range, except for the one between HN_c and j observed in octanoyl- and dodecanoyl-ACP (nomenclature in accordance with Fig. 6*B*). This long range NOE is not observed in holo- or butyryl-ACP and is extremely faint/invisible in tetradecanoyl-ACP. In addition, a few short range NOEs display a decrease in intensity in tetradecanoyl-ACP *i.e.* the NOEs between HN_g and resonances *i*, *f*, and *e*. Supplemental Table 1 lists the chemical shifts for the resonances in the phosphopantetheine arm of the acyl-ACPs. Maximum chemical shift change is observed for HN_c, which changes by 0.11 ppm between holo- and tetradecanoyl-ACP, whereas HN_g displays a chemical shift change of 0.04 ppm. We have modeled the conformation of the phosphopantetheine arm in octanoyl/dodecanoyl-ACP by a slight rotation of bonds using the prosthetic group in the PDB ID 2FAE (crystal structure of decanoyl-ACP of *E. coli*) as a template. As illustrated in Fig. 6*C*, the model satisfies the NOEs observed between HN_c and j as well as NOEs between HN_g and *i*, *f*, *e*, *j*, *j'*. From the data it appears that as two more carbons are added to dodecanoyl-ACP, the arch formed by the phosphopantetheine arm in PfACP widens, resulting in an increase in the space between HN_c and j. Our $^{13}C,^{15}N$-filtered NOESY experiments also point toward the occurrence of multiple conformations of the prosthetic group in butyryl-ACP. NOESY experiments had to be acquired for twice the duration to obtain discernible signal. No NOEs were observed between the acyl chain and the phosphopantetheine arm in any of the acyl-ACPs we studied.

DISCUSSION

P. falciparum is one of the most deadly species of malaria, liable for high rates of mortality in tropical countries. The identification of type II fatty acid synthesis machinery in the apicoplast of the parasite, distinct from the human host, invoked immense interest in understanding the molecular mechanism of fatty acid biosynthesis in the parasite. The observed differences between the host and parasite could lead to the design of drug inhibitors that target the parasite specifically. An indispensable cofactor in this pathway is the acyl carrier protein, which participates in a multitude of biosynthetic pathways that require an acyl transfer step. Acyl carrier protein serves two main functions; (*a*) it protects the fatty acyl chain from the aqueous solvent, and (*b*) it presents the acyl chain to the target

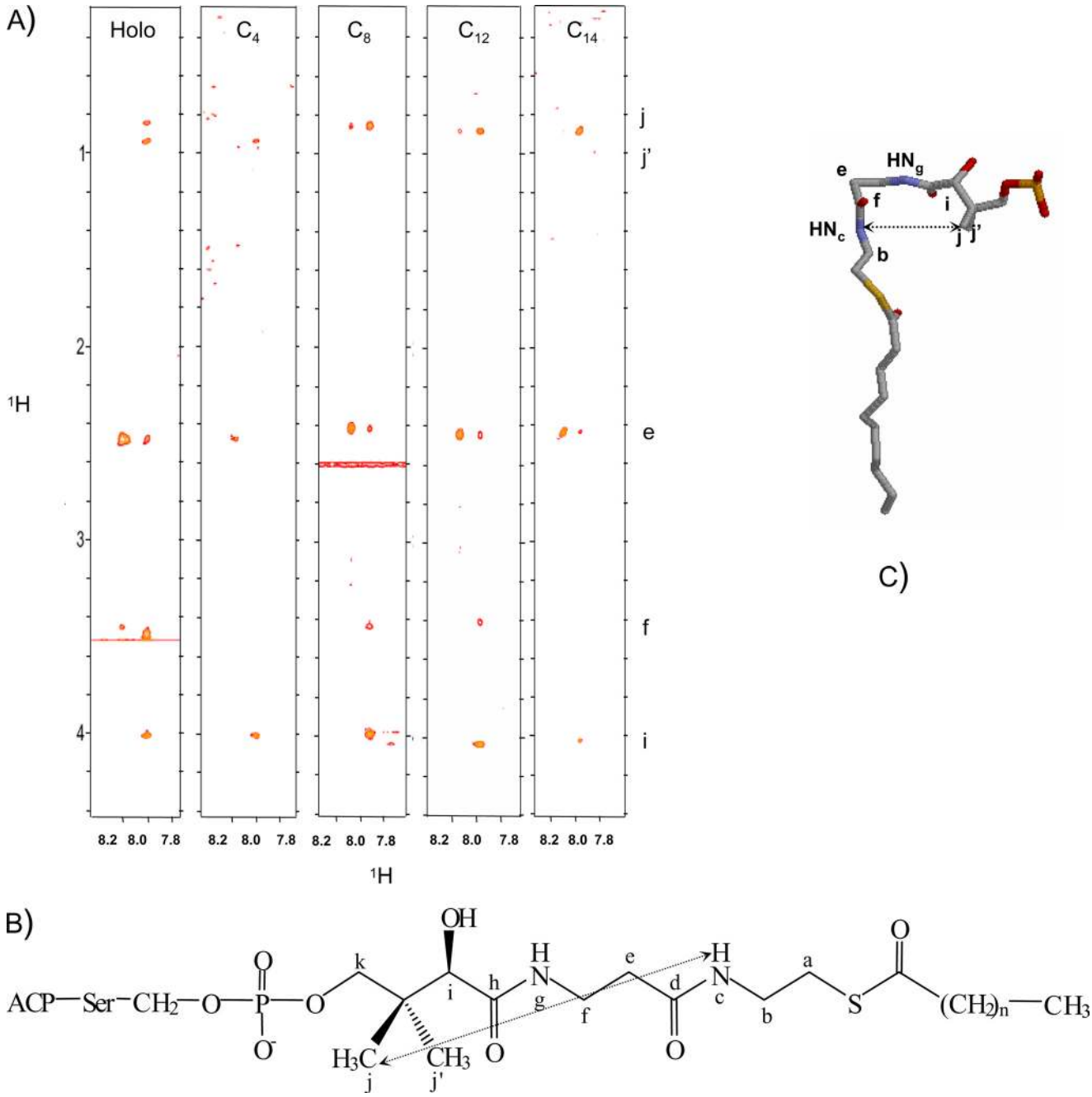

FIGURE 6. **Conformation of the phosphopantetheine arm.** *A*, strips from two-dimensional ^{13}C,^{15}N-double-filtered NOESY spectrum displaying NOEs within the phosphopantetheine moiety in holo-, butyryl-, octanoyl-, dodecanoyl-, and tetradecanoyl-ACP. *B*, structural formula of acylated 4′-phosphopantetheine moiety, where *n* is 3 for butyryl-, 7 for octanoyl-, 9 for decanoyl-, 11 for dodecanoyl-, and 13 for tetradecanoyl-ACP. Atoms of the phosphopantetheine arm have been labeled to correlate with NOEs in the spectrum. An *arrow* shown indicates the long range NOE observed between HN_c and j. *C*, a model illustrating the putative conformation of the phosphopantetheine moiety in PfACP. The model has been generated by slight rotation of bonds in the prosthetic group of decanoyl-ACP of *E. coli* (PDB ID 2FAE) to satisfy the NOEs observed in ^{13}C,^{15}N-filtered experiments in PfACP. The model has been made using RasMol (44).

enzymes and delivers it into their active site. The molecular mechanism by which ACP performs these functions is still unclear. Therefore, we have employed a systematic and comprehensive approach using NMR and a series of acyl intermediates to understand the acyl-PfACP interaction at the molecular level.

Phosphopantetheine Moiety Is Relatively Structured in the Acyl-PfACPs—In PfACP the acyl chain is carried in the hydrophobic core, akin to other members of type II fatty acid pathway (12, 14, 19, 20). The entrance of the hydrophobic cavity is guarded by the side chain of Phe-29, Leu-40 (helix II), Leu-61 (helix III), and Asn-64 (helix IV). The corresponding residues in *E. coli* ACP are Phe-28, Thr-39, Glu-60, and Thr-63 (19). Thr-39 has been regarded as an important residue in stabilizing the polar moieties of phosphopantetheine arm in *E. coli* ACP. In the structures where it has a different conformation, forming an intrahelical hydrogen bond, phosphopantetheine group is disordered (19). Interestingly, in PfACP the position of this residue is flipped with respect to position 30, *i.e.* position 30 is a Thr, and 40 is a Leu, as opposed to a Val and Thr at positions 29

and 39 in *E. coli* ACP and position 31 and 41 in spinach ACP, respectively. The side chains of these two residues lie close in space in the three-dimensional structure of PfACP.

The phosphopantetheine moiety is relatively structured in all acyl-PfACPs we studied, and we were able to obtain NOEs for resonances within the prosthetic group, furnishing structural information on its conformation. This observation is in stark contrast to spinach stearoyl-ACP, where the phosphopantetheine arm was highly disordered, and no NOESY constraints could be observed due to uncertainty in position (14). $^{13}C,^{15}N$ two-dimensional double-filtered experiments acquired with octanoyl- and dodecanoyl-PfACP reveal that the HN_c of the phosphopantetheine moiety is within 5 Å of j (nomenclature is according to Fig. 6*B*), which implies that the methyls of the phosphopantetheine arm face downward, toward the cavity, consistent with the location of Leu-40 in PfACP. Thus, the conformation of the phosphopantetheine arm is slightly different in PfACP compared with *E. coli* ACP, where the two methyls face upward, away from the hydrophobic core, toward Leu-29. The difference in localization of Leu-40 in PfACP compared with *E. coli* and spinach ACP possibly accounts for the more ordered conformation of the prosthetic group, as the hydrophobic interactions between methyls of the prosthetic group and the ACP might restrain it more.

Second Acyl Chain Binding Site in PfACP—Isoleucine 54 is an important residue of ACP in the context of acyl chain interaction (33). In most acyl-ACPs belonging to type II fatty acid biosynthesis pathway, the terminal methyl of the acyl chain points toward the bottom of the core, in close proximity of Ile-54 (19). Consistent with these observations, in PfACP the C_α and C_β carbons of Ile-55 undergo a significant chemical shift change as carbon atoms are added to the ACP molecule. An overall change in chemical shift of Ile-55 by 0.44 ppm in C_α and 2.8 ppm in C_β indicates that the acyl chain approaches the bottom of the hydrophobic cavity. An NOE observed between the terminal methyl of phosphopantetheine moiety and the backbone amide of Phe-51 in octanoyl-ACP confirms that the acyl chain binds a similar site in *P. falciparum*.

Interestingly, in butyryl-ACP no C_α chemical shift change occurs for Ile-55, whereas Phe-29, Ser-37, Leu-40, Ile-44, Lys-62, and Ile-63 display a notable change in chemical shift. The pattern of chemical shift change in butyryl-ACP suggests that the acyl chain has not reached the bottom of the core, and most part of the hydrophobic cavity is still empty. Thus, our chemical shift perturbation studies highlight the presence of an alternate binding site in PfACP, which seems to be occupied by the acyl chain in butyryl-ACP only. A change in HN of Ile-55 is a consequence of the change in side-chain conformation of Glu-48, as disclosed from C_β chemical shift change. Glu-48 O is hydrogen-bonded to Ile-55HN, and hence, chemical shift change is reflected in the HN of Ile-55. These results are in accordance with the crystal structure of *E. coli* I54M mutant of ACP (PDB ID 1L0I), where the tip of the acyl chain lies very close to Leu-42 and Val-43, <4 Å away (19). Interestingly, in a recently published *in silico* study on *E. coli* ACP, the existence of a subpocket II, somewhere between helix I, II, and IV has been suggested, occupied most of the time by the acyl-ACPs in the simulations (21).

Chemical shift changes in octanoyl-ACP casts additional light on the course adopted by the acyl chain inside the hydrophobic core. The tip of the acyl chain progresses from Ile-44 in butyryl-ACP to Ile-55 in octanoyl-ACP, causing slight changes in C_α and C_β of residues Leu-43 and Leu-47. *In silico* studies on *E. coli* ACP have also predicted that the movement of the acyl chain from sub-pocket II to sub-pocket I would necessitate reorientation of Leu-42 (residue corresponding to Leu-43 in *P. falciparum*) and Leu-46 (corresponding to Leu-47) (21). Thus, our solution studies offer experimental proof for a second acyl chain binding site within PfACP.

PfACP Can Hold More Than 10-Carbon-long Acyl Chain in Its Hydrophobic Core—A novel outcome of our work is the revelation that the ACP molecule can house up to 12 carbons in its hydrophobic core, the general agreement being 10 carbons only. This is the first report where the entire series of acyl-ACPs has been structurally characterized and compared, therefore some new observations made in this study are of paramount importance. Moreover, dodecanoyl-ACP has not been structurally characterized in any of the reports to date. It is alluring to compare our results to structural studies on spinach-ACPs. In spinach ACPs, helix packing is different between decanoyl- (C_{10}) and stearoyl-ACP (C_{18}); the distance between helix II and IV is greater in the latter case. A conformational change is observed around helix III that further enlarges the hydrophobic cavity in stearoyl-ACP (13). We observe large C_α chemical shift changes for residues that are present in helix II, loop II, loop III, and helix IV in dodecanoyl-ACP. We conjecture that conformational changes in helix II and loop II would indirectly influence the conformation of helix III. Thus, the differences observed between the two acyl intermediates in spinach ACP might as well be a consequence of a very similar carbon carrying capacity of its ACP.

As all ACPs of type II fatty acid pathway are structurally homologous, similar in size, and in some cases mutually replaceable, they should have a very similar carbon holding capacity. It has been well recognized that the length of a fatty acid chain is determined by the specificity of FAS enzymes, *viz.* fatty acid synthase and thioesterase and not the ACP molecule (34). *E. coli* FAS can synthesize longer chain fatty acids using PfACP (31). Thus, the disparity in products of *E. coli*, spinach, and *P. falciparum* ACP is a consequence of the structural differences in the FAS enzymes and not their ACPs (29).

Given the fact that only 12 carbon atoms can be accommodated in the hydrophobic core, an important question remains regarding the fate of acyl chains with carbons more than 12. In our studies, we notice a slight change in C_α and C_β chemical shift of Ser-37 in tetradecanoyl-ACP, indicating a change in backbone and side-chain conformation of this residue. No chemical shift change is observed for Ser-37 C_α in octanoyl- or dodecanoyl-ACPs. This observation prompted us to speculate that carbon units more than 12 probably protrude out from the top of the PfACP molecule, causing a change in conformation of Ser-37 backbone and side chain. Change in C_β chemical shift of Phe-29 observed in tetradecanoyl-ACP also validates this hypothesis, suggesting a structural change near the top opening of the hydrophobic core. Intramolecular NOE data lend further support to our hypothesis; the phosphopantetheine arm appears to assume an arch-like conformation

in octanoyl- and dodecanoyl-ACP, based on an NOE between HN_c and j (with reference to Fig. 6). This NOE is extremely faint in tetradecanoyl-ACP. We speculate that as two more carbons are added to dodecanoyl-acyl chain, all 14 carbons are not fully protected by the hydrophobic cavity, and therefore, some part of the acyl chain close to the top opening of the hydrophobic core gets exposed to the solvent. This exposure results in widening of the arch formed by the phosphopantetheine moiety and, hence, a change in relative position of HN_c and j. It might as well be possible that the thioester group in the phosphopantetheine moiety would interact with the hydrophilic side chains of residues located at the top opening of PfACP, and thus, the acyl chain experiences push and pull motions, resulting in more than one conformation of the phosphopantetheine arm. The latter possibility seems true, in accordance with the decrease in intensity of NOEs in tetradecanoyl-ACP, observed between HN_g and i, f, and e. In either case, the thioester bond gets exposed to the solvent, resulting in hydrolysis of the acyl chain as observed in $C_{14:0}$ and $C_{16:0}$ PfACP *in vitro*. Hydrolysis could be slowed down only by storing the acyl-ACPs at −20 °C when not in use. The stability of the acyl-ACPs was in the order butyryl > octanoyl > decanoyl > dodecanoyl > tetradecanoyl > hexadecanoyl *in vitro*. Hexadecanoyl-ACP was highly unstable and reverted to holo-ACP completely in less than 2 days, tetradecanoyl-ACP was stable for a week, and dodecanoyl-ACP lasted for nearly a month at 4 °C. Butyryl-ACP was stable for months.

Helix II and Helix III of PfACP Display Strong Electrostatic Repulsion—Our studies unveil another considerably important interaction within the PfACP molecule; that is, the presence of a unique side chain to backbone hydrogen bond that stretches in response to acyl chain elongation. The two residues participating in this bond (Glu-48 O and Ile-55 HN) seem fairly conserved in most ACPs. In the crystal structures of *E. coli* acyl-ACPs, the distance between the N of Ile-55 and the O of Glu-47 does increase in length as a function of acyl-chain elongation. The distance between Ile-54 N and N47 O is 2.69 Å in butyryl-ACP, 2.89 and 2.96 Å in hexanoyl-ACP, 2.87 and 2.93 Å in heptanoyl-ACP, 2.89 Å in decanoyl-ACP, and 2.92 Å for the two molecules present in the asymmetric unit (19). In the spinach stearoyl-ACP structure, the distance between the carboxyl oxygen of Glu-49 and the backbone HN of Val-56 is <2 Å (14). The significance of this bond is not clear; however, we surmise that it plays a role in loop II stabilization. It has already been shown by several groups that Ile-54 is important for the biological function of ACP. Mutation of Ile-54/55 results in loss of fatty acylation of ACP and an increase in the hydrodynamic radii of the molecule (35). We speculate that the hydrogen bond stabilizes this residue, holds the loop in place, and thus, contributes to the overall stability of PfACP. While working with acyl-ACPs, we also observed that as soon as the acyl chain is released from the ACP molecule by thioester bond hydrolysis, the chemical shift value of Ile-55 HN reverts to holo-ACP value of 9.97 ppm, suggesting restoration of the hydrogen-bond length. The observation that hydrogen-bond length increases from butyryl- to tetradecanoyl-ACP sheds light on the state of PfACP molecule, where the lower opening expands to pack as many carbons as possible.

The presence of this hydrogen bond was also confirmed from the pH titration studies with PfACP. Similar sensitivity to pH has been observed in Ile-54 HN of *Helicobacter pylori* as well, suggesting a conserved Glu O-Ile HN hydrogen bond (36). Comparison of the chemical shift value of Ile-55 HN at pH 3.8 (8.27 ppm) when the carboxylate is protonated to that of Ile-55 HN in tetradecanoyl-ACP (8.85 ppm) makes it apparent that the hydrogen bond is still intact in tetradecanoyl-ACP; it only gets longer in response to PfACP expansion. The unusually high pK_a reported by Ile-55 HN for Glu-48 reflects strong electrostatic repulsion in this region that the latter overcomes by upshifting its pK_a value. Assuming a model compound pK_a value of Glu as 4.3, the free energy associated with the upshifted pK_a value of Glu-48 is ~3.6 kJ/mol at 27 °C. A Hill coefficient of 0.81 for the pH titration suggests that the carboxyl pK_a is greater at the high end of pH titration than at the low end. This effect can be explained based only on the presence of carboxyl groups or histidines nearby that also titrate over the same pH range. In PfACP, histidines are not present. Therefore, the unusually high pK_a of Glu-48 can be rationalized based on the NMR structure of PfACP, where the side-chain oxygen atom of Glu-48 is 3.57 Å away from the side-chain oxygen of Asp-59. Interestingly, in most of the ACPs for which we have structural data, a couple of carboxylate side chains lie in close vicinity of Glu-47/48, with their carboxyl group stretching out toward it. For instance, in *E. coli* ACP, the side chains of Glu-53 and Asp-56 lie in the neighborhood of Glu-47 (12). Similarly, in spinach ACP, Asp-57 and Glu-58 lie close to Glu-49 (14). In *Bacillus subtilis* ACP, Glu-47 is present near Asp-48, Asp-51, and Glu-53 (10). In *Mycobacterium tuberculosis* ACP, Glu-52 is very close to Asp-53 and Asp-61 (11). The presence of a hydrogen bond between Glu-47 O and Ile-54 HN and strong electrostatic repulsion in this region between helix II and helix III encompassing residues 47–59 seems to be universal to all ACPs and not a matter of chance in PfACP.

Molecular Mechanism of PfACP Expansion—Our study adds to the present knowledge of acyl chain carriage by ACP molecule and the subsequent transfer of the acyl chain to the active site of the FAS enzymes. A new model emerges elucidating the mechanism of expansion of ACP and its recognition by thioesterase. Butyryl-ACP is the starting point for acyl chain elongation. In butyryl-ACP the acyl chain is in close proximity of Ile-44 and has not penetrated the entire length of the hydrophobic core. As the acyl chain grows, carbon atoms get buried deep in the cavity, causing slight backbone and side-chain conformational changes of Leu-43 and Leu-47 that lie between the two binding sites. A concomitant separation of helix II and helix III occurs because of the strong electrostatic repulsion between carboxylates present in the two secondary structural elements, in conjunction with thrust from inside due to acyl chain packing. These two forces in concert result in outward movement of helix III. Hydrogen bonds and other stabilizing interactions prevent helix III from moving too far from helix II. A conformational change in helix III along with slight changes in other helices generates enough space within the hydrophobic cavity of ACP so as to accommodate acyl chains up to 12 carbon atoms. The x-ray structure of *E. coli* acyl-ACPs (PDB IDs 1LOI, 2FAC, and 2FAE) and spinach (PDB IDs 2FVE, 2FVF, 2AVA, and 2FVA) substantiate our hypothesis; in *E. coli*, the backbone of loop II and helix III, near Ile-54, moves outward in heptanoyl-

and decanoyl-ACP in comparison to butyryl-ACP (19). Similarly, in spinach, the loop between Gly-53 and Asp-57 undergoes conformational change to accommodate long acyl chains (15). The present model also suggests that carbons more than 12 remain outside the hydrophobic cavity and are not fully protected from the solvent. We surmise that the structural differences in the backbone, encompassing loop II and helix III, might be used as a criterion by thioesterase to differentiate the acyl-ACPs. This region is already known to be recognized by a number of enzymes, *e.g.* β-ketoacyl-(ACP) reductase (37, 38), acyl carrier protein synthase (39), protein acyltransferase HlyC (40), acyl-ACP synthetase, UDP-*N*-acetyl glucosamine acyltransferase (41), and β-ketoacyl-ACP synthase III (42). Outward movement of helix III in combination with acyl chain insertion generates strain on the ACP molecule, as revealed from slight changes in C_α and C_β of residues present at the bottom opening of the hydrophobic core in tetradecanoyl-ACP. Thus, the slightest interaction of thioesterase with ACP, which most probably occurs in the region of conformational differences, would trigger the ejection of the acyl chain from the hydrophobic core and thereby lodge it in its own active site.

Conclusions—The present study offers a window into the fatty acid biosynthesis pathway of *P. falciparum*, furnishing details on the mechanism of acyl chain accommodation in the hydrophobic core of PfACP and its recognition by thioesterase. ACP is unique, equipped with features that allow smooth insertion of the acyl chain into the hydrophobic cavity and its delivery into the active site of FAS enzymes. The plastic nature of the hydrophobic core coupled with strong electrostatic repulsion between helix II and helix III facilitate the carriage and release of the fatty acyl chain. Solvent exposure of carbon units in longer acyl-ACPs might further assist the release process by enhancing the dynamics of the acyl chain. Maximum conformational heterogeneity is observed in helix II, loop II, and helix III in the acyl-ACPs we studied. Given the fact that the acyl chain is not sequestered in the hydrophobic core of ACPs of type I pathway (malarial host), this region might serve as a template for inhibitor design to target multiple pathways of the malarial parasite simultaneously.

REFERENCES

1. Lu, H., and Tonge, P. J. (2008) *Acc. Chem. Res.* **41,** 11–20
2. Lu, J. Z., Lee, P. J., Waters, N. C., and Prigge, S. T. (2005) *Comb. Chem. High Throughput Screen* **8,** 15–26
3. Rock, C. O., and Cronan, J. E. (1996) *Biochim. Biophys. Acta* **1302,** 1–16
4. Shen, B., Summers, R. G., Gramajo, H., Bibb, M. J., and Hutchinson, C. R. (1992) *J. Bacteriol.* **174,** 3818–3821
5. Summers, R. G., Ali, A., Shen, B., Wessel, W. A., and Hutchinson, C. R. (1995) *Biochemistry* **34,** 9389–9402
6. Epple, G., van der Drift, K. M., Thomas-Oates, J. E., and Geiger, O. (1998) *J. Bacteriol.* **180,** 4950–4954
7. Kleinkauf, H., and von Döhren, H. (1990) *Eur. J. Biochem.* **192,** 1–15
8. Stein, T., Vater, J., Kruft, V., Otto, A., Wittmann-Liebold, B., Franke, P., Panico, M., McDowell, R., and Morris, H. R. (1996) *J. Biol. Chem.* **271,** 15428–15435
9. Reed, M. A., Schweizer, M., Szafranska, A. E., Arthur, C., Nicholson, T. P., Cox, R. J., Crosby, J., Crump, M. P., and Simpson, T. J. (2003) *Org. Biomol. Chem.* **1,** 463–471
10. Xu, G. Y., Tam, A., Lin, L., Hixon, J., Fritz, C. C., and Powers, R. (2001) *Structure* **9,** 277–287
11. Wong, H. C., Liu, G., Zhang, Y. M., Rock, C. O., and Zheng, J. (2002) *J. Biol. Chem.* **277,** 15874–15880
12. Roujeinikova, A., Baldock, C., Simon, W. J., Gilroy, J., Baker, P. J., Stuitje, A. R., Rice, D. W., Slabas, A. R., and Rafferty, J. B. (2002) *Structure* **10,** 825–835
13. Li, Q., Khosla, C., Puglisi, J. D., and Liu, C. W. (2003) *Biochemistry* **42,** 4648–4657
14. Zornetzer, G. A., Fox, B. G., and Markley, J. L. (2006) *Biochemistry* **45,** 5217–5227
15. Sharma, A. K., Sharma, S. K., Surolia, A., Surolia, N., and Sarma, S. P. (2006) *Biochemistry* **45,** 6904–6916
16. Kim, Y., Kovrigin, E. L., and Eletr, Z. (2006) *Biochem. Biophys. Res. Commun.* **341,** 776–783
17. Evans, S. E., Williams, C., Arthur, C. J., Burston, S. G., Simpson, T. J., Crosby, J., and Crump, M. P. (2008) *Chembiochem* **9,** 2424–2432
18. Płoskoń, E., Arthur, C. J., Evans, S. E., Williams, C., Crosby, J., Simpson, T. J., and Crump, M. P. (2008) *J. Biol. Chem.* **283,** 518–528
19. Roujeinikova, A., Simon, W. J., Gilroy, J., Rice, D. W., Rafferty, J. B., and Slabas, A. R. (2007) *J. Mol. Biol.* **365,** 135–145
20. Wu, B. N., Zhang, Y. M., Rock, C. O., and Zheng, J. J. (2009) *Protein Sci.* **18,** 240–246
21. Chan, D. I., Stockner, T., Tieleman, D. P., and Vogel, H. J. (2008) *J. Biol. Chem.* **283,** 33620–33629
22. Colizzi, F., Recanatini, M., and Cavalli, A. (2008) *J. Chem. Inf. Model.* **48,** 2289–2293
23. Sharma, S. K., Modak, R., Sharma, S., Sharma, A. K., Sarma, S. P., Surolia, A., and Surolia, N. (2005) *Biochem. Biophys. Res. Commun.* **330,** 1019–1026
24. Lambalot, R. H., and Walsh, C. T. (1995) *J. Biol. Chem.* **270,** 24658–24661
25. Delaglio, F., Grzesiek, S., Vuister, G. W., Zhu, G., Pfeifer, J., and Bax, A. (1995) *J. Biomol. NMR* **6,** 277–293
26. Goddard, T. D., and Kneller, D. G. *SPARKY 3*, University of California, San Francisco
27. Sundd, M., Iverson, N., Ibarra-Molero, B., Sanchez-Ruiz, J. M., and Robertson, A. D. (2002) *Biochemistry* **41,** 7586–7596
28. Sundd, M., and Robertson, A. D. (2003) *J. Mol. Biol.* **332,** 927–936
29. Lack, G., Homberger-Zizzari, E., Folkers, G., Scapozza, L., and Perozzo, R. (2006) *J. Biol. Chem.* **281,** 9538–9546
30. Surolia, N., and Surolia, A. (2001) *Nat. Med.* **7,** 167–173
31. Sharma, S., Sharma, S. K., Modak, R., Karmodiya, K., Surolia, N., and Surolia, A. (2007) *Antimicrob. Agents Chemother.* **51,** 2552–2558
32. Clark, A. T., Smith, K., Muhandiram, R., Edmondson, S. P., and Shriver, J. W. (2007) *J. Mol. Biol.* **372,** 992–1008
33. Jones, P. J., Cioffi, E. A., and Prestegard, J. H. (1987) *J. Biol. Chem.* **262,** 8963–8965
34. Chakravarty, B., Gu, Z., Chirala, S. S., Wakil, S. J., and Quiocho, F. A. (2004) *Proc. Natl. Acad. Sci. U.S.A.* **101,** 15567–15572
35. Flaman, A. S., Chen, J. M., Van Iderstine, S. C., and Byers, D. M. (2001) *J. Biol. Chem.* **276,** 35934–35939
36. Park, S. J., Kim, J. S., Son, W. S., and Lee, B. J. (2004) *J. Biochem.* **135,** 337–346
37. Zhang, Y. M., Wu, B., Zheng, J., and Rock, C. O. (2003) *J. Biol. Chem.* **278,** 52935–52943
38. Karmodiya, K., Modak, R., Sahoo, N., Sajad, S., and Surolia, N. (2008) *FEBS J.* **275,** 4756–4766
39. Parris, K. D., Lin, L., Tam, A., Mathew, R., Hixon, J., Stahl, M., Fritz, C. C., Seehra, J., and Somers, W. S. (2000) *Structure* **8,** 883–895
40. Worsham, L. M., Earls, L., Jolly, C., Langston, K. G., Trent, M. S., and Ernst-Fonberg, M. L. (2003) *Biochemistry* **42,** 167–176
41. Gong, H., Murphy, A., McMaster, C. R., and Byers, D. M. (2007) *J. Biol. Chem.* **282,** 4494–4503
42. Zhang, Y. M., Rao, M. S., Heath, R. J., Price, A. C., Olson, A. J., Rock, C. O., and White, S. W. (2001) *J. Biol. Chem.* **276,** 8231–8238
43. Pettersen, E. F., Goddard, T. D., Huang, C. C., Couch, G. S., Greenblatt, D. M., Meng, E. C., and Ferrin, T. E. (2004) *J. Comput. Chem.* **25,** 1605–1612
44. Sayle, R. A., and Milner-White, E. J. (1995) *Trends Biochem. Sci.* **20,** 374–376